Analysis on Nano-Aluminum Combustion Behaviour

Authors

Bonizzoni	Umberto	10723223	umberto.bonizzoni@mail.polimi.it
De Salvo Fontoura	Isabella	11031090	isabella.desalvo@mail.polimi.it
Lemes Gribel Soares	João	10988472	joao.lemes@mail.polimi.it
Nesticò	Diego Giovanni	10599952	diegogiovanni.nestico@mail.polimi.it
Robert	Joseph Noel Kiren	10974257	josephnoel.robert@mail.polimi.it

Abstract

Introduction: The aim of this report is to analyze nano-sized aluminum powders combustion for solid propellant formulations, in order to understand which characteristics of the powders can alter the burning rate, achieving better ballistic performances. Four different powders are provided and analyzed, both micro-sized and nano-sized: μAl3, nAl01j, nAl18a and nAl19a.

Methods: SEM and TEM images are provided, in order to perform an analysis of the powders micro structure. Thermogravimetric data are used to assess the powders reactivity through a pre-burning characterization, while actual burning rate measurements, for different solid propellant formulations, are used to directly analyze the ballistic behaviour described by Vielle's law.

Results: As predicted, nano-sized aluminum powders display higher reactivity and lead to faster burning solid propellants, when compared to micro-sized formulations. An explanation for different combustion behaviours between nano-sized aluminum powders has been proposed, related to the alumina shell thickness, the powder specific surface area and the particle sizes distributions.

Nomenclature

Al_2O_3	Alumina	DTA	Differential Thermal Analysis	SEM	Scanning Electron Microscopy
Al	Aluminum	HTPB	Hydroxyl-terminated Polybutadiene	I_{sp}	Specific Impulse
AP	Ammonium Perchlorate	D_{43}	Mean Diameter, Volume-Weighted	S_{sp}	Specific Surface
a_s	Average Particle Size	μAl	Micro-sized Aluminum	TEM	Transmission Electron Microscopy
C_{al}	Content of Aluminum	nAl	Nano-sized Aluminum	TG	Thermogravimetry

1 | Introduction

In solid rocket propulsion, aluminum powders are widely employed in propellant formulations as an energetic fuel and combustion stability enhancer [1]. Recently, a significant amount of research has been directed to nano-sized aluminum powders, which due to their high specific surface area, present significantly higher reactivity parameters when compared to micro-sized aluminum, the latter being more widely used in commercial applications.

The aforementioned increased reactivity together with a change in the particle burning mechanism (aggregation-controlled, as opposed to agglomeration-controlled in the case of μAl) have been shown to significantly enhance the burning rate of solid propellants employing nAl, as well as decrease the associated ignition delay [2].

However, while the enhanced reactivity of nAl may provide some attractive characteristics for certain particular applications, it also presents some related drawbacks. Due to the smaller average diameter, the nano-sized powder has a smaller active metal content, since the passivation layer of aluminum oxide (usually of constant thickness) represents a larger total mass fraction of the material. This attribute leads to a reduced performance of the solid propellant (in terms of theoretical I_{sp}), as the proportion of the active energetic metal content in the formulation is decreased. Additionally, storability concerns may arise lowering even more the aluminum content of the powder in improper environments, as shown by accelerated ageing experiments [3].

The aim of the present work is to perform a concise but comprehensive analysis on nano-aluminum powders, with a focus on reactivity characterization and effects on burning behavior. Reactivity parameters will be computed for powder batches provided by different providers, according to the method proposed by Ilyin et. al [4]. Electron microscopy images will be provided for the studied material in order to allow for a qualitative assessment of the disperse powder characteristics. Following that, standardized thermoanalytic techniques such as DTA and TG will be performed on the powder as a pre-burning characterization, in order to identify thermal decomposition phenomena and allow for a general overview on the reaction behavior. Finally, in order to assess the actual influence the aluminum particle size will have in the burning behavior of a given propellant, ballistic data from a strand burner will be analysed for propellant samples prepared with the different aluminum powders, and burn rate coefficients estimated in accordance to the semi-empirical Vielle's law.

2 | Powder Characterization

For this study, one μAl powder and three different nAl powders are taken into account, whose physical characteristics are shown in table 1. The actual content of aluminum, as predicted by a volumetric technique [5], is significantly lower for nAl powders when compared to μAl3. This is due to the presence of a thin aluminum oxide shell which covers the surface of nAl powders during passivation, and represent a proportionally larger volume for smaller particles.

ID	$C_{Al}[wt.\%]$	D_{43} $[\mu m]$	$S_{sp}[m^2/g]$	a_s $[nm]$
Al3	99.5 ± 0.7	44.4	< 0.1	-
Al01j	85.9 ± 0.8	0.138	12.6 ± 0.1	176.4 ± 1.4
Al18a	84.6 ± 0.6	0.140	16.9 ± 0.1	131.5 ± 0.8
Al19a	79.7 ± 0.6	0.141	15.8 ± 0.1	140.6 ± 0.9

Table 1: Aluminum powders characterization

In fig. 1, obtained by SEM imaging, μAl particles shapes are shown. Note that particles are mostly spheroid, and with some exceptions, characterized by small clustering, which is defined as an agglomeration of particles; moreover the particles surface morphology is relatively smooth. Indeed the reduced specific surface area in micro aluminum particles helps in clustering prevention, since it decreases the number of active sites where particles can interact and stick together. A lower specific surface area means fewer surface atoms are available to form bonds with other particles, thereby minimizing the tendency to agglomerate [6].

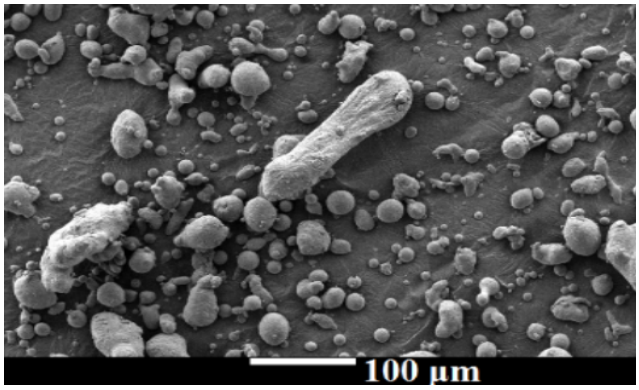

Figure 1: SEM of μAl3

Concerning the nAl powders, as can be visualized in fig. 2, the thin alumina shell can be spotted using SEM imaging, and is recognizable as the lightest region surrounding each particle of the aluminum powder. Indeed, since aluminum presents a higher electron density compared to alumina, it presents itself as darker in the SEM imaging energy beam. This detail can provide interesting insights into combustion performance prediction of aluminum powder, by enabling the estimation of the oxide layer thickness, which provides protection and stability to the Al powder, and the particle surface morphology, as rougher surfaces can affect combustion due to the presence of irregularities that act as points of initiation of the reaction [7].

A larger lighter region, hence a thicker alumina shell, indicates a reduced pure Al content in the particles.

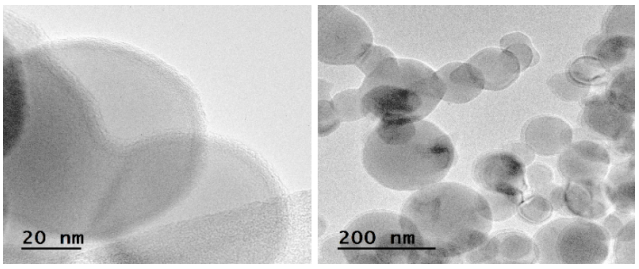

Figure 2: TEM of nAl01j (left) and nAl18a (right)

In fig. 3, SEM images are shown. SEM scans the sample surface with a focused beam of electrons, usually in vacuum, providing information about the topography of the sample. Secondary electrons (i.e. electrons generated due to ionization by other forms of radiations) are also detected. From the SEM images provided, it can be noted that, for the nAl sample on the left, the particles are mostly spherical or spheroid-shaped, with a uniform size distribution. A tendency of the particles to cluster together, owing to the fact that specific surface area of nAl is considerably higher than the one of μAl3, can also be noted. Clustering increases the effective surface area enhancing the reactivity, resulting in a more rapid and strong combustion, due to the increased heat release [8].

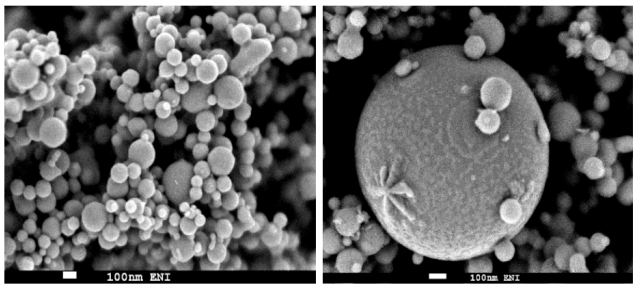

Figure 3: SEM of nAl01j (left) and nAl18a (right)

On the other hand, for the nAl sample shown on the right, a larger particle can be noticed, in the micrometric range, with other nanoparticles lumped around it. This observation may indicate the presence of outliers or non-uniformities in this sample particle size distribution.

3 | Reactivity Analysis

With the structure of the available powders characterized, it is possible to proceed with their reactivity analysis, by means of a post-processing of data acquired through a thermogravimetric analyzer. During the trial, the samples are placed inside a furnace with a temperature and pressure-controlled environment. A balance continuously measures the mass of the sample, while the temperature is increased over time. In the present work, all experiments were performed with a fixed heating rate of 10 K/min and the gas present in the environment was air, in order to allow for the characterization of the oxidation behavior of the powders.

In the following discussion, TG and DTA curves will be shown, while the evaluated reactivity parameters [4] are presented in table 2 and hereby stated:

- T_{bo} - Temperature of oxidation onset
- α_1 - Degree of transformation at 660°C
- α_2 - Degree of transformation at 1100°C
- v_{ox} - Maximum oxidizing velocity
- $T_{v_{ox}}$ - Temperature for which v_{ox} is reached

In order to evaluate the oxidation onset temperature, Piloyan's tangent method was implemented [9]. For μAl, the pre-exponential factor and the activation energy, present in the Arrhenius equation, were retrieved for pure aluminum from [10], considering the high amount of pure aluminum inside the particles, as previously discussed. Meanwhile, for nAl, Arrhenius' parameters were evaluated through an experimental method based on the thickness of the alumina shell surrounding the particles, as described in [11]. However, this approach resulted not sufficiently precise to match the differences between nAl powders, at least when compared to the ones observed in the experimental TG traces.

	μAl3	nAl01j	nAl18a	nAl19a	Unit
T_{bo}	879.2	741.9	769.2	732.8	$[K]$
α_1	0.99	26.31	30.36	22.07	[%]
α_2	4.93	63.32	66.71	56.75	[%]
v_{ox}	0.0195	0.174	0.206	0.116	$[\mu g/min]$
$T_{v_{ox}}$	1246	880.5	855.6	854.7	$[K]$
$t_{Al_2O_3}$	25.18	3.064	2.515	3.654	$[nm]$

Table 2: Calculated reactivity parameters of the powders

Initially, it's possible to discuss μAl3 aluminum behaviour, for which TG and DTA traces are shown in fig. 4.

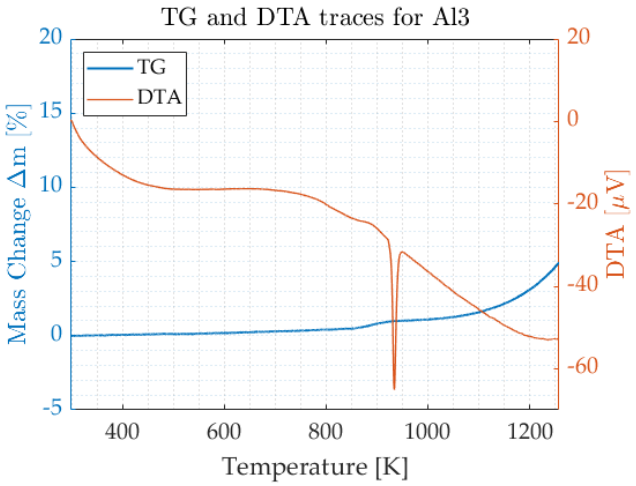

Figure 4: Thermogravimetry traces of powder μAl3

As can be observed, a relatively flat TG trace is registered, up to an evaluated temperature of 879.2K for which a slight initial mass gain is recorded. This is followed by an endothermic peak at a temperature around 933.5K, corresponding to the point at which the aluminum metal melts. At this point, after the melting process, which starts cracking the oxide layer, a slow oxidation process begins, associated to a mass gain and a linear DTA trace. Indeed, the maximum oxidizing velocity is only computed at a temperature of 1246K, the last registered sample, indicating that the process is still going on while the machine is shut down.

The slowness of the reaction is also reflected in the degrees of transformation α_1 and α_2: at 660°C almost no difference in mass is recorded, while at 1000°C only a five percent variation is reached. It can be concluded that μAl3 undergoes oxidizing only after the aluminum melts, hence the reaction is described by a heterogeneous slow and moderate oxidation between liquid aluminum and air.

A significantly different behaviour is observed with nAl, compared to μAl, as presented in fig. 5 for the oxidation record of powder nAl01j. As will be described, this is mainly due to the nature of the alumina shell which covers nAl particles, leading to a dynamic oxidation process.

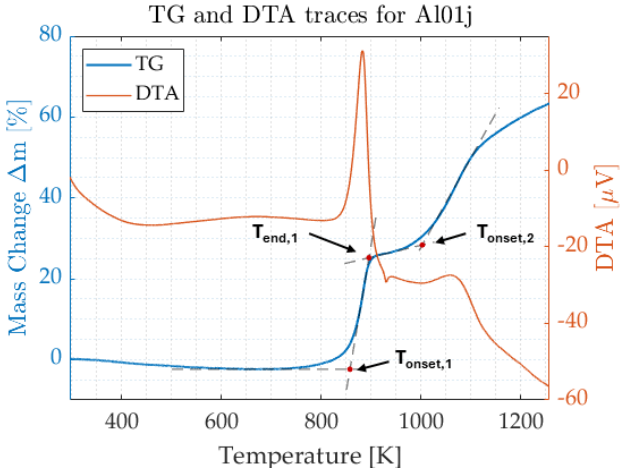

Figure 5: Thermogravimetry traces of powder nAl01j; experimental data related to DTA/TG number 108.

The reaction onset is faster and begins at lower temperature, as shown in fig. 5 and evaluated by the reaction parameters exposed in table 2. The main difference is the presence of two separated oxidation stages: the first one happens before the aluminum melting point, mainly due to the phase change of the alumina shell from amorphous to γ-crystalline structure, while the second one happens when the less-dense liquid aluminum pushes the alumina shell, cracking it in different spots where oxidation occurs.

In fig. 6, a comparison of the TG traces for the three given nAl is presented: the general behaviour is the same, however some differences can be spotted. First of all, nAl18a and nAl19a, which have a greater S_{sp}, seem to start oxidizing at around the same temperature, which is lower compared to nAl01j. The intensity of the oxidation seems related to the equivalent thickness of the alumina shell. Indeed nAl18a, which has the thinnest alumina shell among the three powders, exhibits the most intense oxidation process, for both first and second oxidation stage, as evaluated in table 2 and shown in fig. 6, followed by nAl01j and consequently nAl19a. The latter phenomenon could be explained since a thinner (on average) alumina shell is easier to break.

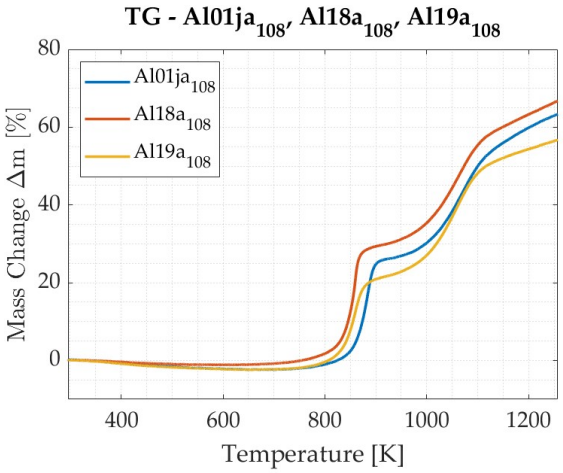

Figure 6: Thermogravimetry traces for different nAl powders; experimental data related to DTA/TG number 108.

4 | Burning Characterization

For each of the four different aluminum powders, experimental burning rate data were taken for three solid propellant compositions, varying the proportions between AP and metal (binder fraction remained the same due to processing concerns). The nomenclature for each propellant strand is as follows: the first two numbers following AP represent the percentage of coarse AP particles, while the following two refer to the percentage of fine AP. The number following Al represents the percentage of aluminum present in the mixture. The evaluated burning rate coefficients of Vielle's law, obtained by curve fitting, are reported in table 3:

		Al8		Al4
		AP6510	AP7500	AP8200
μAl3	a	1.2591	0.8745	1.0954
	n	0.4392	0.5026	0.4728
nAl01j	a	1.4803	1.4560	1.4103
	n	0.5534	0.4976	0.5269
nAl18a	a	1.6372	1.5173	1.4182
	n	0.4838	0.4889	0.5232
nAl19a	a	1.5502	1.4760	1.2709
	n	0.5161	0.4938	0.5631

Table 3: Vielle's law burning rate coefficients

In fig. 7 burning rate is shown as a function of pressure, for three different propellant compositions containing μAl3. It is clear that for higher pressures the mixture burns faster (as expected for AP/HTPB propellants), since a reduced flame height leads to a smaller residence time and decreases the size of agglomerates, allowing for their ignition to occur closer to the propellant surface. The highest burning rate is achieved when AP is in a bimodal form, since the presence of fine particles (around 20μm) are more suitable to fill the spaces between coarse particles (around 200μm), which allows for combustion to occurs also inside the pockets and prevents the formation of large condensed combustion products (CCPs) which, in general, decrease the burn rate. In other words, a propellant with unfilled space available between large oxidizer grains allows for agglomeration of the heated molten metal, favoring the appearance of large Al agglomerates which reduces their specific surface area, their reactivity and consequently the burning rate. From this, it can be summarized that the combustion behavior for μAl particles is to melt, agglomerate and then oxidize.

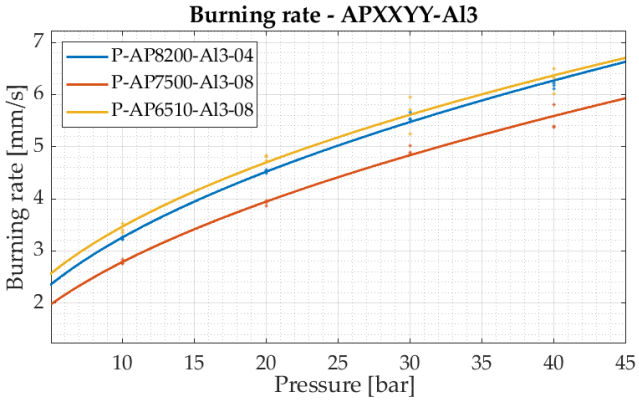

Figure 7: Burning rate of three different propellants with μAl3: AP8200-Al04, AP7500-Al08, AP6510-Al08.

To be noted, the bimodal AP6510 formulation results not only in a better burning rate compared to the unimodal AP7500, but also higher (even if slightly) when compared to the more oxidizer rich formulation AP8200. Besides, bimodal propellant formulations tend to enjoy better theoretical packing and ease of processability.

In fig. 8 burning rates are shown for four propellant compositions with same AP/Al ratios, but employing different samples of the aluminum powders. The bimodal AP was chosen for the comparison, since the presence of fine AP increases the effect of the aluminum particle size, enhancing the difference between nAl powders.

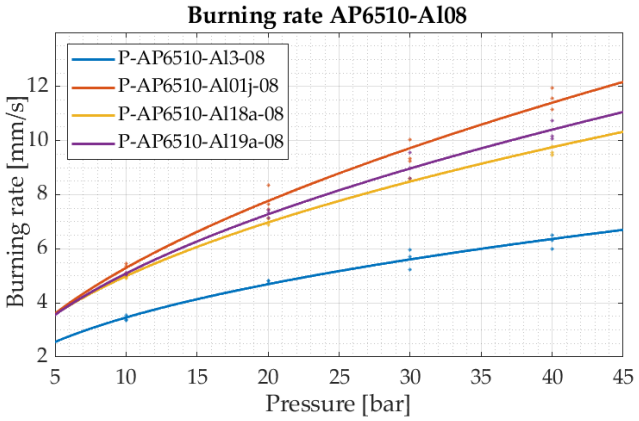

Figure 8: Burning rate comparison between propellants with μAl and nAl, for AP6500-Al08 formulation.

As expected, the high reactivity of nAl results in a higher burning rate, which is around two times faster compared to μAl, at equal pressure. In general, particles of nAl powders tend to form partially premixed oxidized flakes (see fig. 9), called aggregates, which are able to finish oxidation

and completely combust still at (or very close to) the propellant surface layer, with a significant energy and heat release. This difference happens in part due to the aluminum oxidation process that takes place before the melting point, as observed in the TG analysis. From this mechanism, some hints arise on how different characteristics of the nAl powders can be reflected in the combustion behaviour.

It can be noted, however, that propellants prepared in the same ratios but with different batches of nAl have a slight difference in burning behavior which appears to be statistically significant, even though they nominally have very similar average particle sizes (based on the De Brouckere mean diameter D_{43}). Paradoxically, the burning rate of the propellants seem to be inversely correlated with the specific surface area (S_{sp}) of their respective powders. Some of the data related to the experimental powder characterization of each of the batches might provide some insights into this phenomena.

As shown in Tab. 2, based on the measurements of aluminum content and specific surface area of the powder, an alumina shell thickness may be estimated assuming all the particles have spherical shape and are of same size. The alumina shell around particles have been shown to be consistently on the range of 3-4nm (unless the powder is aged), and therefore any significant deviation from this domain might indicate either a wider particle size distribution or a prevalence of particles of different shapes. Indeed, the nAl18a powder presents a calculated oxide thickness of around 2.5nm, which could indicate the presence of some amount of larger particles (in the micrometric range) skewing the above value. The SEM image discussed in 3 corroborates with this hypothesis. The bulk of the nano-aluminum powder must have a smaller average particle diameter (since D_{43} is maintained), which increases the total powder S_{sp}. However, the fraction of larger particles introduce a combustion mechanism associated with the formation of large metal agglomerates that stick to the propellant surface, just like in μAl, reducing the ballistic performance.

5 | Conclusion

In the present work, an analysis on the combustion behavior of aluminized composite solid propellants has been performed, showing that the presence of nano-aluminum increases the burning rate when paired with the usual AP/HTPB formulations. This is in-line with the thermal decomposition results obtained by applying techniques such as thermogravimetry to the metal powder themselves.

Moreover, under certain circumstances, namely the presence of fine AP in the propellant composition, differences in the burning behavior can be observed between propellants employing different batches of nAl. These have been hypothesized from powder characterization and microscopic imagery to be resultant from the powder's particle shape and size distributions, which affects the incidence of the aggregation and agglomeration mechanisms on the propellant surface. Future work should consist on further studies focusing on clarifying the effect of powder dispersity on condensed combustion products characteristics.

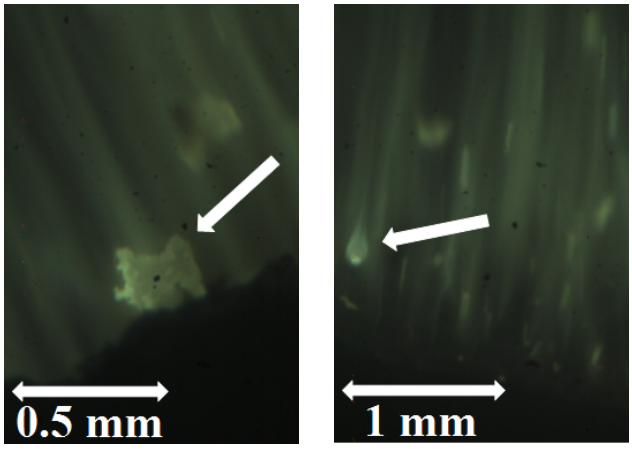

Figure 9: Burning visualization of P-AP6510-Al01j-08 (left) and P-AP8200-Al019a-04 (right) propellants.

References

[1] EW Price. Combustion of metalized propellants. *Progress in Astronautics and Aeronautics*, 1984.

[2] L. DeLuca, L. Galfetti, G. Colombo, F. Maggi, A. Bandera, V. Babuk, and V. Sinditskii. Microstructure effects in aluminized solid rocket propellants. *Journal of propulsion and power*, 26(4):724–733, 2010.

[3] C. Paravan, A. Verga, F. Maggi, and L. Galfetti. Accelerated ageing of micron-and nano-sized aluminum powders: Metal content, composition and non-isothermal oxidation reactivity. *Acta Astronautica*, 158:397–406, 2019.

[4] A. Ilyin, A. Gromov, V. An, F. Faubert, C. de Izarra, A. Espagnacq, and L. Brunet. Characterization of aluminum powders i. parameters of reactivity of aluminum powders. *Propellants, Explosives, Pyrotechnics*, 27:361–364, 2002.

[5] C. Liang, S. Wulin, Lv Jie, C. Xia, and X. Changsheng. Research on the methods to determine metallic aluminum content in aluminum nanoparticles. *Materials Chemistry and Physics*, 120(2-3):670–675, 2010.

[6] G. Wang, H. Wang, Q. Cui, X. Li, X. Wu, H. Liao, and Z. Zhang. Synthesis, analysis, and characterization of aluminum nanoparticles coated with 2,2,4-trimethylpentane. *Metals*, 13(2):322–344, 2023.

[7] F. Zheng, L. Wang, S. Zhang, L. Zhang, Q. Hu, and L. Wang. Specific surface area evolution and shrinkage and control of pre-sintered nickel clusters. *Metals*, 12(10):1693–1704, 2022.

[8] T. M. Klapötke. Energetic materials. *Advanced Materials*, 18:2245–2264, 2006.

[9] V. M. Gorbachev. A method for determining the starting temperature of the thermal effect. *Thermal Anal.*, 19, 1980.

[10] S. Hasani, M. Panjepour, and M. Shamanian. Oxidation and kinetic analysis of pure aluminum powder under nonisothermal condition. 2022.

[11] A.B. Vorozhtsova, M. Lernerb, N. Rodkevichb, H. Niec, A. Abrahamc, M. Schoenitzc, and E.L. Dreizin. Oxidation of nano-sized aluminum powders. *Thermochimica Acta*, 636:48–56, 2016.